Received September 1999
Revised May 2000
Accepted May 2000

# Finite element simulation of transient laminar flow past a circular cylinder and two cylinders in tandem

## Influence of buoyancy

B.S.V. Patnaik
*Department of Computational Science, NUS, Singapore*
P.A.A. Narayana
*Department of Applied Mechanics, IIT, Madras, India, and*
K.N. Seetharamu
*Department of Mechanical Engineering, USM, Perak, Malaysia*

***Keywords*** *Cylinders, Buoyancy, Finite element simulation, Computational fluid dynamics*

***Abstract*** *Flow past an isolated circular cylinder and two cylinders in tandem is numerically simulated, under the influence of buoyancy aiding and opposing the flow. A modified velocity correction method is employed, which has second order accuracy in both space and time. The influence of buoyancy on the temporal fluid flow patterns is investigated, with respect to streamlines, isotherms and streaklines. Comparisons are made with respect to mean center line velocities, drag coefficients, Strouhal number and streakline patterns. Degeneration of naturally occurring Kármán vortex street into a twin eddy pattern is noticed in the Reynolds number (Re) range of 41-200, under buoyancy aided convection. On the contrary, buoyancy opposed convection could trigger vortex shedding even at a low Re range of 20-40, where only twin eddies are found in the natural wake. Temporal evolution of unsteady eddy patterns is visualized by means of numerical particle release (NPR). Zones of vortex shedding and twin vortices are demarcated on a plot of Richardson number against Strouhal number. Root mean square (RMS) lift coefficients ($C_{L,RMS}$) and average drag coefficient ($\overline{C_d}$) are obtained as a function of Richardson number (Ri).*

## Nomenclature

| | | | |
|---|---|---|---|
| $\underline{C}$ | = Courant number $U\Delta\tau/\Delta X$ | $Pe_c$ | = cell Peclet number ($U\Delta X/\nu$) |
| $\overline{C}_{d1}$ | = average drag coefficient of the upstream cylinder | Pr | = Prandtl number ($\nu/\alpha$) |
| | | Re | = Reynolds number ($U_\infty D/\nu$) |
| $\overline{C}_{d2}$ | = average drag coefficient of the downstream cylinder | Ri | = Richardson number ($Gr/Re^2$) |
| | | St | = Strouhal number ($f_{VS}D/U_\infty$) |
| $C_{L,RMS}$ | = root mean square lift coefficient | t | = time |
| D | = diameter of the circular cylinder | $T_{PS}$ | = time period of shedding |
| $f_{vs}$ | = vortex shedding frequency | u | = velocity in the stream wise direction (X-direction) |
| Gr | = Grashof number ($g\beta\Delta\theta D^3/\nu^2$) | | |
| p | = static pressure | U | = non-dimensional velocity in X-direction ($u/U_\infty$) |
| $p_\infty$ | = free stream pressure | | |
| P | = non-dimensional pressure ($p/\rho U_\infty^2$) | $U_\infty$ | = free stream velocity |

International Journal of Numerical Methods for Heat & Fluid Flow, Vol. 10 No. 6, 2000, pp. 560-580.


The authors thank the referees for their invaluable suggestions.

v = velocity transverse to the streamwise direction (Y-direction)
V = non-dimensional velocity in Y-direction ($v/U_\infty$)

*Greek*
$\alpha$ = thermal diffusivity of the fluid
$\beta$ = coefficient of thermal expansion
$\Delta\tau$ = incremental time step
$\Delta X$ = grid size in X-direction
$\theta$ = non-dimensional temperature
$\theta_\infty$ = non-dimensional temperature of the cylinder surface
$\nu$ = kinematic viscosity
$\tau$ = non-dimensional time (t.U(/D)
$\nabla$ = gradient operator

*Acronyms*
CFD = computational fluid dynamics
FEM = finite element method
MVCM = modified velocity correction method
NPR = numerical particle release
N-S = Navier Stokes
R-K = Runge-Kutta
RMS = root mean square
SEVP = stabilized error vector propagator

## 1. Introduction

The phenomenon of vortex shedding, which bears the name of the celebrated aerodynamicist, Theodre von Kármán, has application to a wide variety of thermal, fluid flow and vibration related problems. The present state of understanding has been enriched by a vast number of experimental, analytical and computational studies. The problem of flow past a circular cylinder has received considerable attention due to its fundamental significance and the wide engineering relevance. Simulating the transient nature of the vortical structures forms an acid test for any numerical algorithm. The background and evolution of literature can be found in Berger and Wille (1972), and more recently in Williamson (1996). Flow past an isolated circular cylinder has applications in the field of constant temperature anemometry, where the sensor wire or film is maintained at a certain temperature above the fluid stream. Knowledge of heat transfer coefficients is certainly invaluable to designers in the development of instruments using wires such as thermo elements and hot wire anemometers (Eckert and Soehngen, 1952).

Vortices that are shed from a single cylinder or two cylinders are severely influenced by the buoyant forces, apart from the viscous and inertial effects. The phenomenon of vortex shedding has implications in applications such as heat exchanger tubes, nuclear reactor fuel rods, cooling towers, chimney-stacks, offshore structures, cooling of electronic equipment, etc. All these configurations come under the broad classification of bluff bodies, where a circular cylinder is one of the basic elements. Bluff body wakes are complex as they involve the interaction of three shear layers, viz. boundary layer, separating shear layer and the unsteady wake (Williamson, 1996). A study of the mechanisms associated with laminar flow past a circular cylinder forms the first step towards understanding the vastly more complicated phenomenon of turbulence (Eaton, 1987).

Flow past tube bundles is a logical extension of cylinders in tandem and transverse arrangements. There exists a dynamic interaction between the shed vortices in the wake and the circular configuration. Hence, the resultant wake behavior is entirely different from that behind an isolated circular cylinder. Also, the Reynolds numbers associated with these flows is very high. However,

a scaled down version of this more complicated tube bundle problem is that of flow past two cylinders in tandem. Though most of the practical applications fall in the Reynolds number (Re) range of $10^3$ to $10^5$, the low Re range (20 to 200) assumes significance owing to its ease in computability. Numerical simulation of flow and forces for high Re range has not been achieved due to lack of a good turbulence model which can accurately simulate the wake and the turbulent vortex street (Slaouti and Stansby, 1992). Classical experiments of Slaouti and Gerrard (1981) have pointed out that some aspects of large-scale wake behavior associated with vortex shedding are similar in the low Re range (i.e. 100 to 200) and in the high Re range ($10^3$ to $10^5$). For two cylinders in tandem, Igarashi (1982) has shown the effect of eddy mechanics on the longitudinal spacing between the cylinders. Zdrakovich (1977) and Ohya *et al.* (1989) have given excellent reviews on the wake interference effects.

Chang and Sa (1990) have applied a finite difference based stabilized error vector propagator (SEVP) scheme to study the vortex shedding mechanisms in the near wake of a heated/cooled single circular cylinder. Hatanaka and Kawahara (1995) have obtained the critical value of Grashof number, when the flow changes from a periodic to a twin vortex pattern for Re = 100, under the influence of buoyancy aided convection. Vortex shedding behind a circular cylinder was numerically simulated by a velocity correction method in Patnaik *et al.* (1996), with a focus on the analysis of near wake mechanisms. However, from the existing literature, it is not known if the phenomenon of vortex shedding could be triggered in the low Re range of 20 to 40, where the natural wake contains only twin vortices. Also, investigations have not reported how an additional force due to buoyancy is likely to influence the vortex structure of two cylinders in tandem. Further, to gain a better insight into the associated fluid flow characteristics, an analysis of the temporally evolving wake pattern assumes significance. Unsteady external flows with transients should receive greater attention in convective heat transfer due to the increasingly greater use of automatic control devices in the high performance heat exchanger industry (Shah, 1981). Hence, an accurate regulation of the fluid flow, its more precise evaluation, and an understanding of the thermal transients will have far reaching ramifications in the evolution of new designs. The present study is an attempt to address these issues by solving full Navier-Stokes equations with a modified velocity correction algorithm. Numerical particle release (NPR) technique is incorporated, which assists in the better visualization of the temporally evolving simulated wake patterns.

## 2. Mathematical formulation

### *2.1 Governing equations*

The governing partial differential equations are mass, momentum and energy conservation, applicable for two-dimensions. The flow is assumed to be two-dimensional, laminar, incompressible and Boussinesq approximated. These equations, in their non-dimensional form, can be written as:

$$\frac{\partial U}{\partial X} + \frac{\partial V}{\partial Y} = 0; \tag{1}$$

$$\frac{\partial U}{\partial \tau} + U\frac{\partial U}{\partial X} + V\frac{\partial U}{\partial Y} = -\frac{\partial P}{\partial X} + \frac{1}{Re}\left(\frac{\partial^2 U}{\partial X^2} + \frac{\partial^2 U}{\partial Y^2}\right) + Ri\theta; \tag{2}$$

$$\frac{\partial V}{\partial \tau} + U\frac{\partial V}{\partial X} + V\frac{\partial V}{\partial Y} = -\frac{\partial P}{\partial Y} + \frac{1}{Re}\left(\frac{\partial^2 V}{\partial X^2} + \frac{\partial^2 V}{\partial Y^2}\right); \tag{3}$$

$$\frac{\partial \theta}{\partial \tau} + U\frac{\partial \theta}{\partial X} + V\frac{\partial \theta}{\partial Y} = \frac{1}{Re\,Pr}\left(\frac{\partial^2 \theta}{\partial X^2} + \frac{\partial^2 \theta}{\partial Y^2}\right). \tag{4}$$

where:

$$X = x/D;\ Y = y/D;\ U = u/U_\infty;\ V = v/U_\infty;\ \tau = tU_\infty/D;\ P = p/\rho U_\infty^2. \tag{5}$$

Here, D is the cylinder diameter, with $U_\infty$ and $P_\infty$ referring to the free stream velocity and pressure, respectively.

Unlike reality, only a finite computational domain can be employed in numerical simulations. Hence, it is important to locate the in-flow, far-field and out-flow boundaries sufficiently far away from the system under investigation such that the boundary conditions do not introduce significant undesirable effects. As regards the boundary conditions applied over the computational fluid flow domain, in-flow and far-field boundaries were specified with a free stream velocity ($U = U_\infty = 1.0$; $V = 0.0$). No-slip, no-suction, no-blowing ($U = V = 0.0$) is enforced on the cylinder surface(s). The downstream exit boundary is located at 30D, which does not influence the vortices formed in the near wake of the cylinder. Out-flow boundary conditions are natural ones that arise in the context of the finite element method applied to the Navier-Stokes equations. The following homogeneous Neumann boundary conditions are applied at the out-flow boundary,

$$-P + \frac{1}{Re}\frac{\partial U}{\partial X} = 0.0; \quad \frac{1}{Re}\frac{\partial V}{\partial Y} = 0.0.$$

These boundary conditions were implemented in a weak fashion rather than in a point-wise manner. Non-dimensional temperature ($\theta_\infty$) for the freestream is imposed as 0.0, while that on the cylinder surface ($\theta_c$) is 1.0. However, for the sake of clarity and simplicity in computations, heating or cooling of the cylinder surface is taken care of only by the directional influence of the buoyant forces, which is included in the X-momentum equation. Richardson number ($Ri = Gr/Re^2$; Gr refers to the Grashof number, and Re to the Reynolds number) is positive or negative, depending on whether the cylinder is heated or cooled. There exists a coupling between the momentum and energy equations, which necessitates their simultaneous solution. The influence of a buoyant force,

either aiding or opposing the flow direction, is investigated. The three Reynolds numbers employed in the present study are 40, 100 and 200. The fluid flow simulations are carried out, within the Boussinesq approximation range of Ri = –1.0 to +1.0.

*2.2 Numerical approach*

The algorithm employed in the present study is a modified velocity correction method (MVCM) of Ren and Utnes (1993), which is essentially an extension of the popular projection scheme of Chorin (1968), proposed in the finite difference context. This was extended to finite elements by Donea *et al.* (1982). Here, the time integration is based on Runge-Kutta (R-K) mid-point procedure, which is second order accurate. Spatial discretization is performed by the finite element based Galerkin weighted residual formulation with linear triangular elements. Discretization of the fluid flow domain is performed by a simple and popular iso-parametric mapping procedure of Zienkiewicz and Phillips (1971). Grid fineness is carefully achieved such that a fine mesh results in regions such as no-slip and wake, in order to resolve the gradients better. Furthermore, a powerful automatic renumbering scheme of Collins (1973) is incorporated, which greatly reduces storage space and computing time.

The underlying philosophy behind the scheme can be explained as follows. To start with, pressure terms of the momentum equations are ignored and the fictitious velocities are obtained. Of course, these velocity values will not satisfy the continuity equation. A correction is applied to the velocities after solving the pressure Poisson equation. Consequently, the energy equation is solved to obtain the temperatures. Thus, an iterative scheme is set up. The present investigation employs a Galerkin weighted residual formulation, which essentially employs shape functions as the weighting functions. The finite element shape functions are available in Fletcher (1984) and Segarlind (1984). Detailed formulation is available in Patnaik (1998).

*2.3 Numerical aspects*

In time marching schemes, time step ($\Delta\tau$) governs the stability of the algorithm. Here, the value of the time step depends on the choice of the mesh size and the velocity distribution at that instant in time. In the present scheme, stability of the algorithm is governed by the advection-diffusion term in the equation for the velocity prediction phase. Thus, the time step ($\Delta\tau$) is obtained by:

$$C < \left\langle \frac{Pe_c}{2 + Pe_c} \right\rangle,$$

where Courant number (C) = U. $\Delta\tau/\Delta$X and the cell Peclet number ($Pe_c$) = U.$\Delta$X/$\nu$. Here, $\Delta\tau$ and $\Delta$X refer to the minimum time step and grid spacing in

the X-direction, respectively, while "$\nu$" refers to the kinematic viscosity of the fluid. Reduction in the incremental error between two successive iterations is taken as the criterion for convergence. As the present simulation procedure leads to a steady periodic solution, the iterative process ceases after obtaining about 25 to 30 vortex shedding cycles.

An assessment of the accuracy of the numerical simulation procedure is, of course, of fundamental importance. It is essential to confirm that the numerical simulation constitutes the desirable representation of the governing partial differential equations. To this end, three types of grid densities have been chosen to check for the self-consistency of the present study. The discretization process involves a certain amount of error, which can be systematically reduced by a series of grid refinements. The grids chosen are:

(a) 1,464 nodes; 2,872 elements;

(b) 2,124 nodes; 4,298 elements;

(c) 2,568 nodes; 5,476 elements.

The results showed a maximum difference of about 4-6 percent in Strouhal numbers and average drag coefficients between (a) and (b) type grids, while the variation between (b) and (c) type grids was about 2-3 percent. In the light of this observation, (b) type mesh density was found to give sufficient accuracy with modest computational time, and hence selected for the simulation study.

## 3. Results and discussion

### *3.1 Single circular cylinder*

Simulation of complex, temporally evolving fluid flow patterns behind a circular cylinder is a challenging task. Validation of the numerical scheme is an important part of any CFD study. To start with, the computational algorithm is used to describe the near wake at early instants in time, which is also known in the literature as the impulsive start. Centerline velocities when the evolution of fluid flow reaches a non-dimensional time ($\tau$) equal to 3.0, are given in Figure 1, which represent the downstream near wake. Experimental results of Bourd and Coutanceau (1980) and numerical simulations of Chilukuri (1987) are also presented. Here, the wake region immediately behind the circular cylinder has a region of reverse flow.

*3.1.1 Streamlines*. An understanding of the temporal evolution of the instantaneous fluid flow patterns associated with the flow past a circular cylinder has a bearing on the overall analysis. A sequence of streamline patterns are depicted in Figure 2, for Re = 40 and Ri = –1.0. The flow is symmetrical and resembles potential flow character (Figure 2a). With progress in time, flow separation occurs at around $\tau$ = 4 (Figure 2b) and two small stationary eddies are formed in the downstream wake region. These eddies are fed by circulation from the shear layers and grow in size, with time. For $\tau$ = 9, the two attached, symmetrical eddies of opposite circulation (Figure 2c) can be noticed. They grow further in size, along and across the stream, and result in a

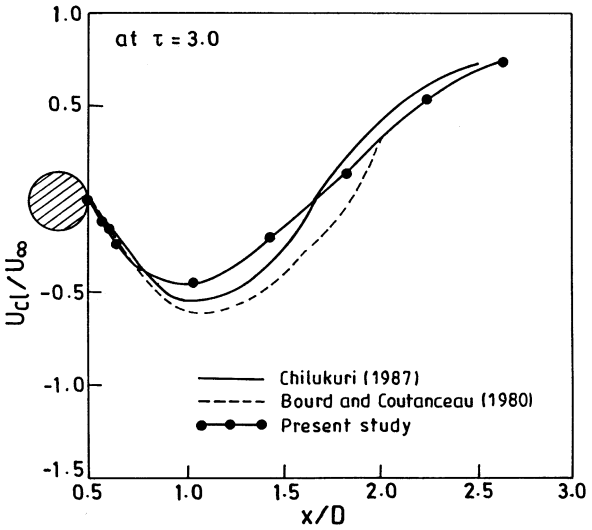


**Figure 1.**
Comparison of the mean centreline velocity ($U_{cl}/U_\infty$) behind the circular cylinder at $\tau = 3$

wake, which is much wider and longer, as against what is generally perceived for natural shedding. However, after reaching sufficient concentration, further supply of circulation from the shear layers (to the growing eddies) is cut off. Buoyancy also causes this initial pair of eddies to move forward, and into the far wake (Figure 2d), without any symmetry breaking bifurcation. However, another pair of eddies is in the process of formation (Figure 2e) in the near wake. Here, the absence of sinuous nature of the flow, in the far downstream, should be particularly noticed. With further progress in time, a steady periodic pattern is established with a serpentine motion and a definite periodicity. The eddy formation and its washing away into the wake can be seen in Figure 2(f). The numerical flow visuals depicted in Figures 2(g) and 2(h) are at a half vortex shedding cycle apart. Thus, from the temporally evolved patterns, it can be observed that, for Re = 40 and Ri = –1.0, vortex shedding is triggered, unlike the existence of twin eddies in a natural wake for Ri = 0.0.

*3.1.2 Isotherms.* An isotherm is a constant temperature contour, and hence manifests the movement of heat flow at a specific instant of time. Thermal boundary layer growth starts symmetrically from the forward stagnation point and becomes thicker towards the aft. Beyond the point of boundary layer separation, the region of influence (due to the cylinder surface) is a function of Richardson number. The temporal evolution of isotherms is depicted in Figure 3 for Re = 40 and Ri = –1.0. Here, the isotherms also exhibit a periodic movement, depicting the oscillatory nature of the wake region. In these sequence of plots, the evolution of the twin standing eddies into a vortex roll-up process is well represented. Further, it should be pointed out that $\tau$ = 105 and $\tau$ = 110, which are at half vortex shedding cycle apart, represent the corresponding isotherms (Figures 3d and 3e), against the streamline patterns in Figures 2(g) and 2(h). On the upstream side, the distribution is regular and

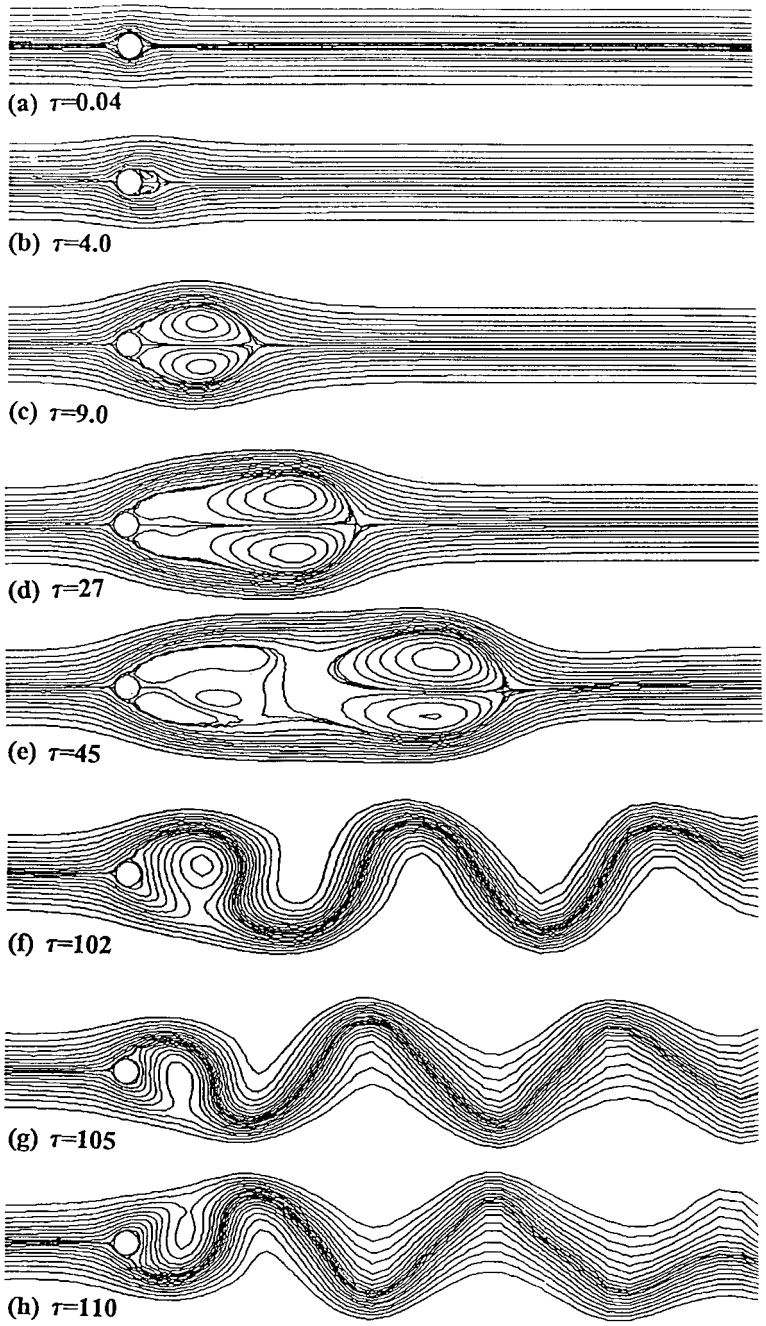


**Figure 2.**
Temporal evolution of streamlines for Re = 40; Ri = –1.0

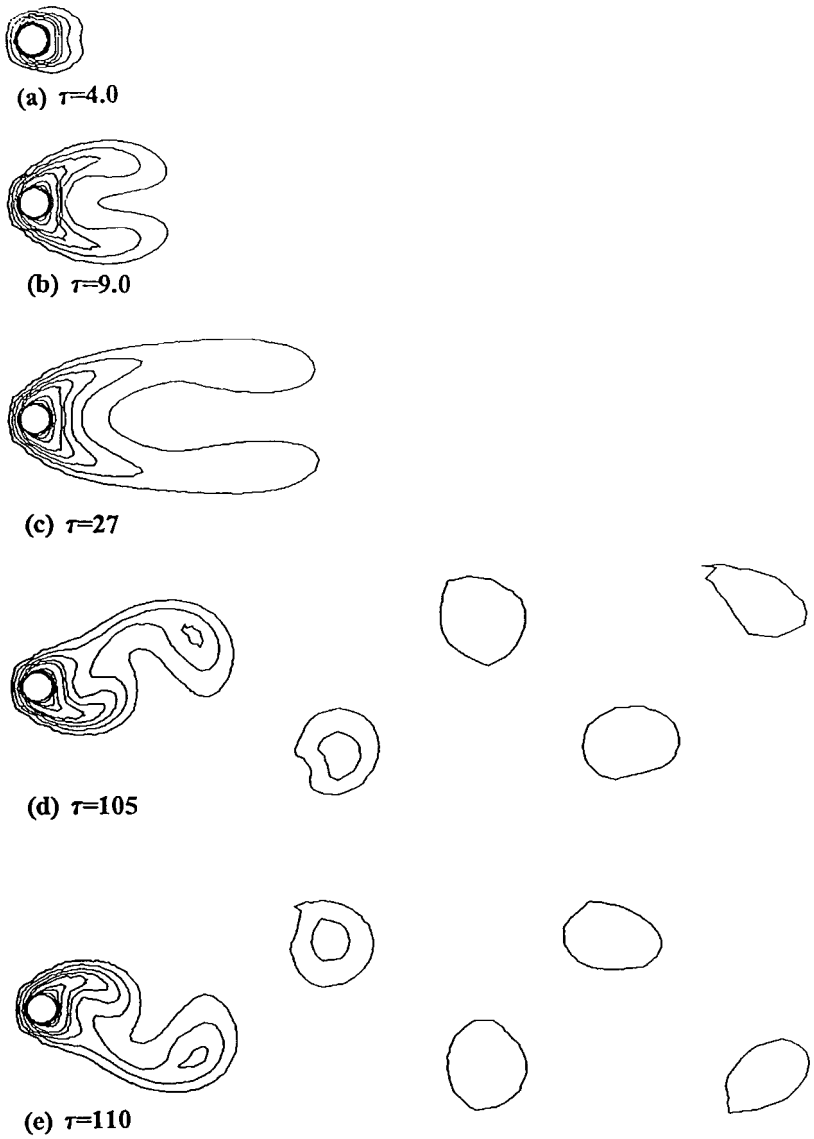


**Figure 3.**
Temporal evolution of isotherms for Re = 40; Ri = –1.0

packed, while in the downstream the influence of vortex shedding on the isothermal patterns can be clearly perceived from the migration of heat flow lines.

*3.1.3 Streaklines*. Streamlines and isotherms have a limited capability to truly represent the spatio-temporal history of the wake. A sequence of instantaneous plots is essential to understand the unsteady nature of the flow. Owing to this, a simple methodology is proposed and implemented to obtain the streaklines. Experimental flow visualization techniques typically employ

various physical tracers, such as hydrogen bubbles, tufts, oil films, smoke particles, dye, etc. (Visualized Flow, 1988). The present investigation closely emulates this tracer technique and employs numerical particle release (NPR). The problem of tracer getting diffused with the main flow is a common sight in an experimental visualization, while NPR is devoid of such an undesirable interaction with the main flow.

Streakline visuals are obtained by the simultaneous release of particles from about 15 to 20 distinct and suitably chosen locations. Particles are released at regular intervals over a specific period of time, until they represent a qualitative streakline picture, depicting the wake structure. The bookkeeping strategy is a node based elemental connectivity, which was highly beneficial in the reduction of search time. The novel element of the present approach is that of a simple search philosophy. This comprises the following steps:

(1) Search for the new location of the released particle within the same element in which it was released.

(2) Search the immediate neighbors of the element.

(3) Its further neighbors and so on . . . This novel search reduction strategy saves an enormous amount of computing time.

However, the particle will cease to exist once it crosses the out-flow boundary.

A typical streakline pattern obtained by NPR is shown in Figure 4, depicting the structure of the wake for a natural shedding case against an experimental visualization from Visualized Flow (1988). In their experiments, the Kármán vortex street behind a circular cylinder was realized by means of an electrolytic precipitation and the white curves are streaklines. The vortex pattern associated with natural shedding is very well represented in the numerical prediction against the experimental visual. The distinct feature is the gradual roll-up of the shear layers at crests and troughs and also the fact that there is a mutual connection between the shed eddies through a trail streakline, which essentially originates in the near wake. By means of a number of instantaneous streamlines and experimental flow visuals, Perry *et al.* (1982) have shown that every shed eddy is ultimately interconnected to every other eddy by its own "umbilical cord" or "thread".

An analysis of the wake zone aerodynamics reveals that the influence of buoyancy is diametrically different under "aided" and "opposed" convection. When the direction of buoyancy opposes the flow, velocity in the wake region is reduced. Its consequence are:

- separation points move towards the upstream;
- strength of the shear layer increases;
- eddy roll-up process gets more activated.

A detailed temporal sequence of the streakline patterns under the influence of buoyancy opposed convection is presented in Figure 5, for Re = 40 and Ri = – 1.0. Figure 5(a) represents the initial locations of particles for the generation of

(a) Experimental visual (Visualized Flow, 1988)

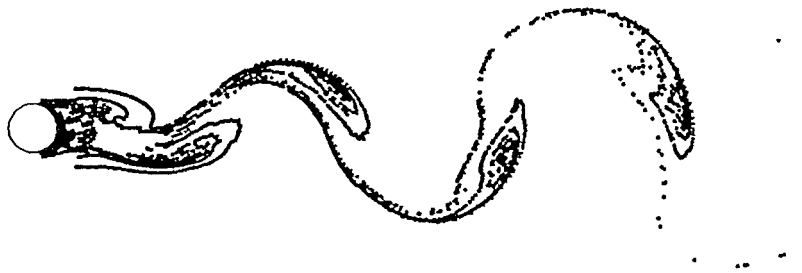

(b) Numerical visual by NPR

**Figure 4.**
Comparison of streakline patterns with an experimental visual

streaklines. The evolution of vortex shedding process is captured and the movement of these eddy conglomerations into the downstream can be observed in Figures 5(b) to 5(d). The undulating nature of eddies during the evolution process should be particularly noticed. A fully evolved version of the streakline plot is shown in Figure 5(d).

*3.1.4 Strouhal number*. The wavy and sinuous nature of the downstream wake region could be noticed from the streamlines, streaklines and isotherms. These undulations of this serpentine motion are measured by Strouhal number (St) = $f_{vs}D/U_{\infty}$. Where $f_{vs}$ is the vortex shedding frequency, D is the diameter of the circular cylinder, and $U_{\infty}$ refers to freestream velocity. In Figure 6, Strouhal number is plotted as a function of both Reynolds and Richardson numbers. While heating accelerates the boundary layer formed on the cylinder surface and hastens the vortex shedding process, cooling impedes the rate of eddy roll-up. Beyond a certain value of Richardson number only twin vortices are seen instead of a vortex street. This was observed experimentally by Noto and Matsumoto (1985), and the process is known as the "breakdown of the Kármán vortex street". The numerical flow visuals of Hatanaka and Kawahara (1995) have established that, for a Reynolds number of 100, the vortex shedding process ceases at Ri = +0.125. The corresponding value obtained in the present

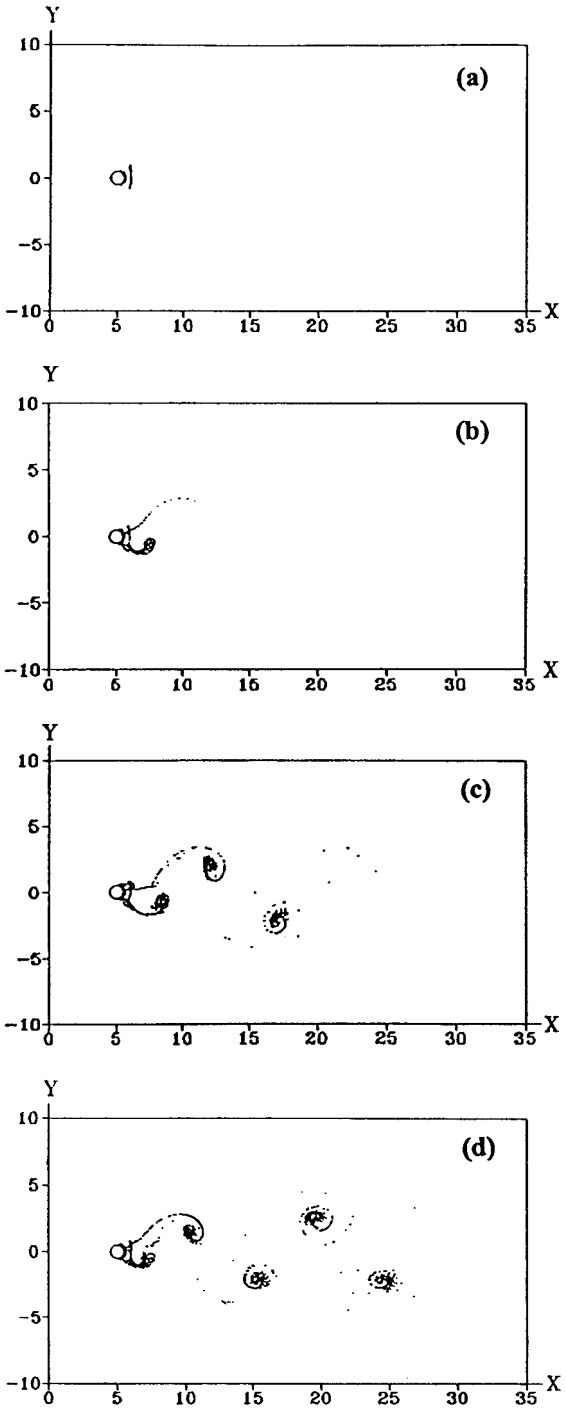


**Figure 5.**
Temporal evolution of streakline patterns for Re = 40; Ri = –1.0

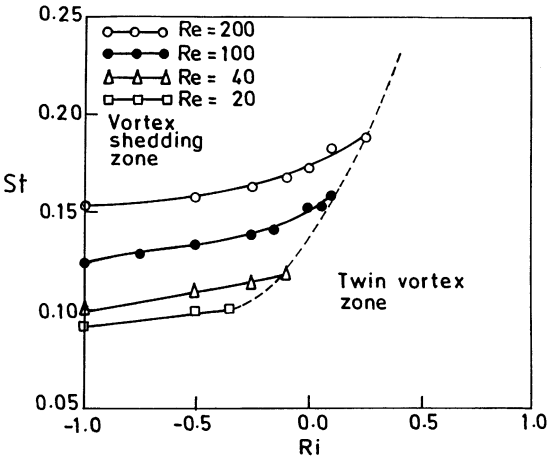


**Figure 6.**
Demarcation of vortex shedding and twin vortex zones

investigation is Ri = +0.12, which is in good conformity with the earlier investigation. The two zones due to vortex shedding and twin eddies are clearly demarcated in Figure 6. This demarcation is a typical case of Hopf bifurcation, where in a steady state solution branches off into a periodic phenomenon. It implies that all branches of steady state and periodic solutions meet along the boundary dividing the two zones. While a steady state solution exists, towards the right of the boundary (twin vortex zone), it is marked by a periodic phenomenon on the left (vortex shedding zone).

*3.2 Two cylinders in tandem*

*3.2.1 Numerical flow visuals*. In this section, results pertaining to the flow past two cylinders in tandem at twice the diametrical pitch are presented. Two quasi-periodic eddies are formed in the gap region between the cylinders (Zdrakovich, 1977). In the absence of a buoyant force, the downstream wake region of the second cylinder is marked by the formation and shedding of vortices, over the Re range of 41 to 200. However, only a pair of symmetrical attached stationary eddies are normally present, between Re = 20 to 40 (pure forced convection). The aim of the present section is to study the influence of buoyancy aided or opposed convection on these shed eddies.

Streamlines are shown in Figure 7 for Richardson numbers in the range of –1.0 to +1.0, after attaining either steady or steady periodic states. Vortex shedding can be prominently seen from the upstream cylinder, with a wide wake in the downstream for Ri = –1.0 (Figure 7a). An intense fluid dynamical activity should be particularly noticed in the gap region between the cylinders. On the contrary, vortex shedding is totally suppressed under buoyancy driven convection, from both the cylinders for Ri = +1.0 (Figure 7f), while it persists even at Ri = +0.10 (Figure 7d). Isotherms, presented in Figure 8, are crowded on the upstream half of the first cylinder, indicating a high radial heat flux. The distribution is regular and packed on the upstream and

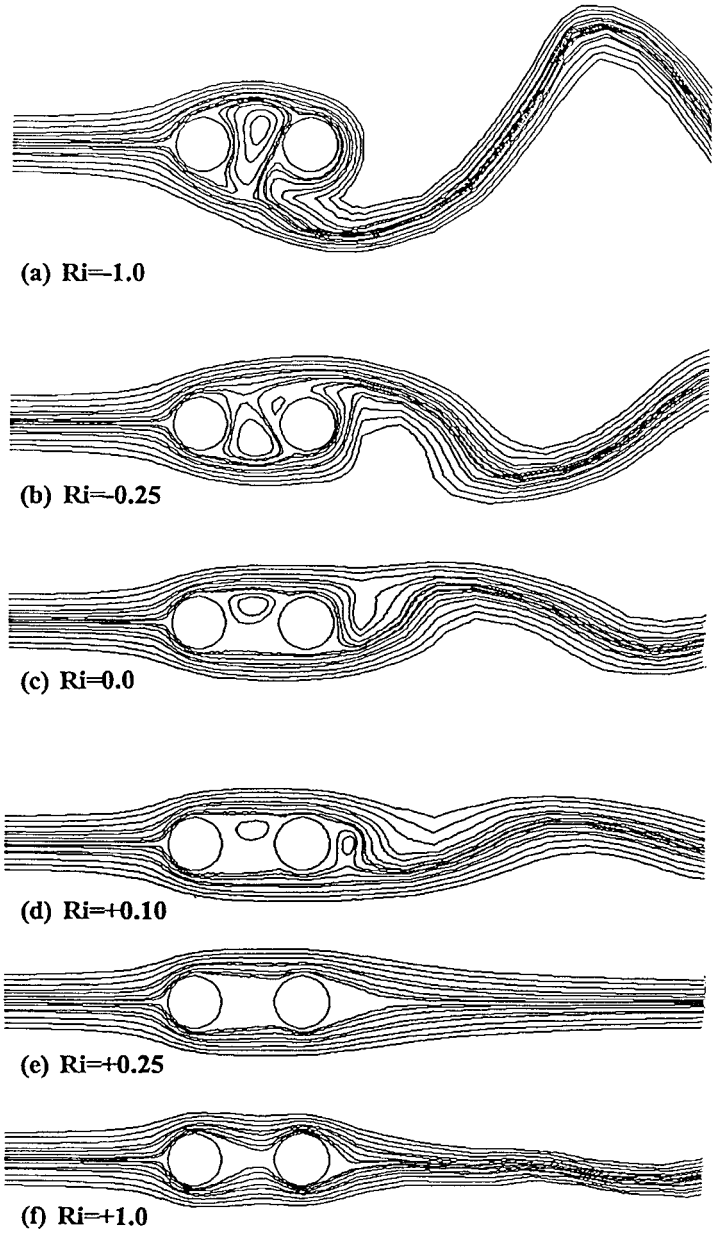


**Figure 7.**
Streamlines for Re = 100

is independent of the fluid flow patterns in the gap region or the downstream. A higher diffusion of heat flow can be observed for buoyancy opposed convection, while the zone of influence is smaller for aided convection cases. NPR is employed to obtain the wake structures, as depicted in Figure 9. Here, vortex shedding activity is intense for Ri = –0.5 (Figure 9a), while the vortex

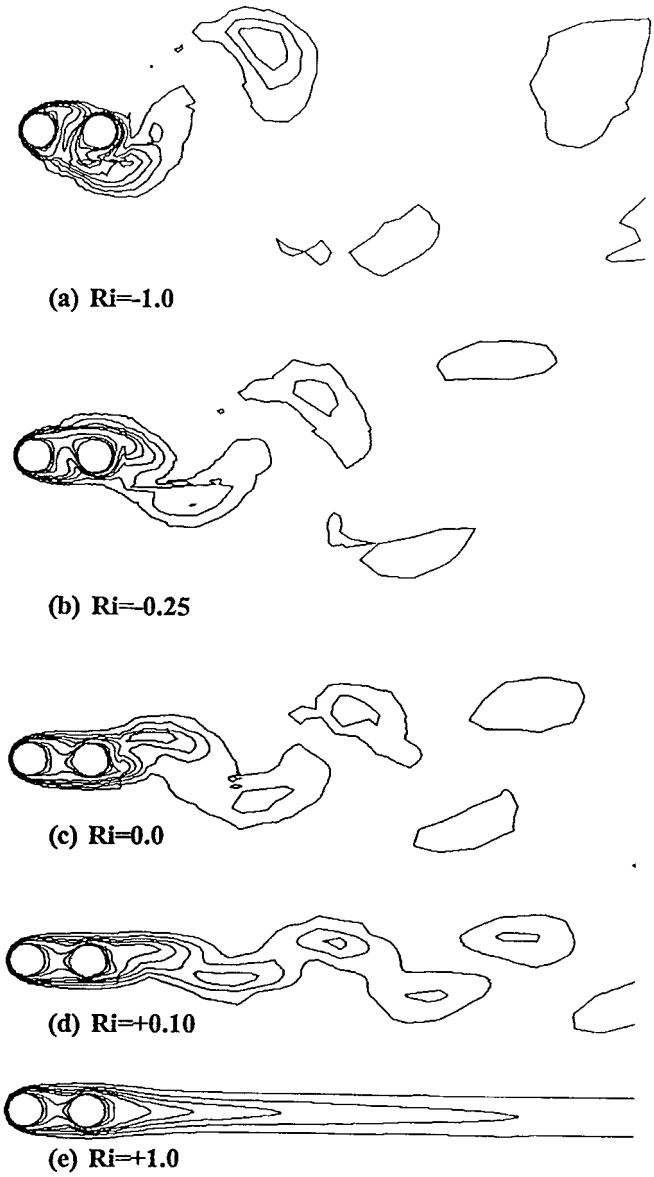


**Figure 8.**
Isotherms for Re = 100

street is totally suppressed for Ri = +0.50 (Figure 9c). The connection between eddies can be noticed for Ri = 0.0 (Figure 9b) by means of a trail streakline.

*3.2.2 Lift and drag.* Shear and pressure contributions are integrated to obtain the temporal lift and drag histories. Drag coefficient values are averaged over ten vortex shedding cycles to obtain the values of $\overline{C}_{d1}$ and $\overline{C}_{d2}$. RMS values are deduced from the temporal lift coefficient fluctuations. A

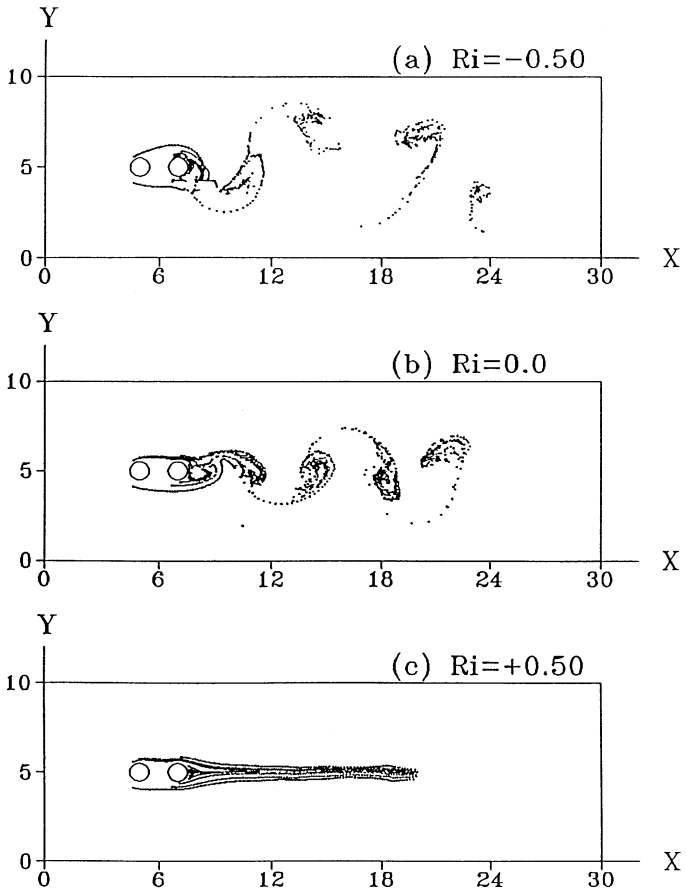


**Figure 9.**
Streaklines for Re = 100

comparison of drag coefficients is given in Table I for Ri = 0.0. The agreement is reasonable for the upstream cylinder, while the variation is large for the downstream cylinder. Drag coefficient of the upstream cylinder has a value almost equal to the flow past an isolated circular cylinder. The resistance offered by the rear cylinder decreases, as it is submerged in the wake of the upstream cylinder. This wake shading influence partially justifies the lack of unanimity between the two numerical simulations, with respect to the downstream cylinder drag. Further, Stansby and Slaouti (1993) have pointed out variations in the prediction of forces among various numerical schemes, in connection with flow past an isolated circular cylinder.

| Reference | Upstream cylinder | Downstream cylinder |
|---|---|---|
| Slaouti and Stansby (1992) | 0.89±0.05 | −0.21±0.15 |
| Present study | 1.138±0.05 | −0.05±0.03 |

**Table I.**
Comparison of average drag coefficient ($\overline{C}_{d1}, \overline{C}_{d2}$) for Re = 200

Average drag coefficient as a function of Richardson number is presented in Figure 10. Owing to heating (i.e. under buoyancy aided convection), for Re = 40, $\overline{C}_{d1}$ increases with increases in Ri, but remains almost flat for Re = 100 and 200. This dichotomy may be attributed to the following. For Re = 40, under pure forced convection (i.e. Ri = 0.0), two standing eddies are formed behind both the cylinders. When the flow is aided with buoyancy, separation points move towards the aft. For Re = 40, drag contribution due to skin friction increases substantially, while savings due to pressure drop decrease marginally. The sum of these two components, which comprises the total drag, increases. On the contrary, for Re = 100 and 200, eddy roll-up process persists in the wake region under pure forced convection. The points of separation shift towards the downstream and upstream side of the cylinder under buoyancy driven and opposed convection respectively. In the latter case, there is a wide wake, which causes the drag coefficient value to increase substantially for the upstream cylinder. However, the overall trends for the downstream cylinder drag ($\overline{C}_{d2}$) have shown similarity for Re = 40, 100 and 200. Here, due either to heating or to cooling, average values of $\overline{C}_{d2}$ have increased, in comparison with pure forced convection.

RMS lift coefficient values plotted in Figure 11 have shown a similar trend for both the cylinders. Owing to vortex shedding, periodic lift forces are induced, which is essentially dictated by the wake zone aerodynamics. From the temporal lift coefficients, time period of vortex shedding ($T_{PS}$) is obtained.

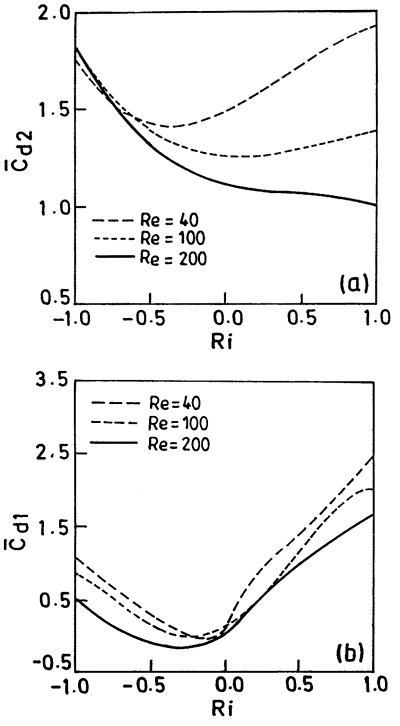


**Figure 10.**
Variation of average drag coefficiency against Richardson number (Ri) (a) upstream cyclinder (b) downstream cylinder

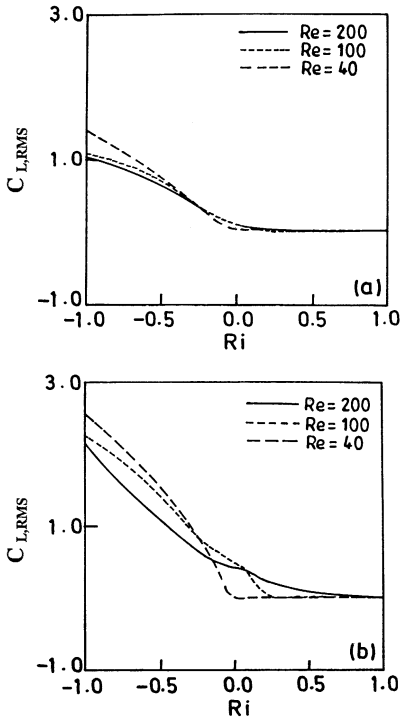


**Figure 11.**
Variation of root mean square (RMS) lift coefficient against Richardson number (Ri) (a) upstream cyclinder (b) downstream cylinder

Vortex shedding frequency ($f_{VS}$) and hence Strouhal number (St) are deduced from this. Table II presents a comparison of Strouhal number against the results of Slaouti and Stansby (1992) for Ri = 0.0. Figure 12 is a plot of Richardson number against Strouhal number. Beyond a certain value of Ri, vortex shedding degenerates into two standing eddies, marking the breakdown of the Kármán vortex street. As can be observed, this value of Ri is different for both the upstream and downstream cylinders. The two zones, viz. due to vortex shedding and twin vortices, are demarcated separately for both cylinders.

## 4. Summary and conclusions

The influence of "buoyancy" aided or opposed convection on the flow past a circular cylinder and two cylinders in tandem is numerically investigated. A modified velocity correction procedure with Runge-Kutta (R-K) time integration, and an FEM based Galerkin weighted residual formulation are employed for the simulation. Temporal evolution of the wake patterns is simulated by means of streamlines, isotherms and streaklines. The structure of

| Reference | Upstream cylinder | Downstream cylinder |
|---|---|---|
| Slaouti and Stansby (1992) | 0.13 | 0.13 |
| Present study | 0.137 | 0.137 |

**Table II.**
Comparison of Strouhal number (St) for Re = 200

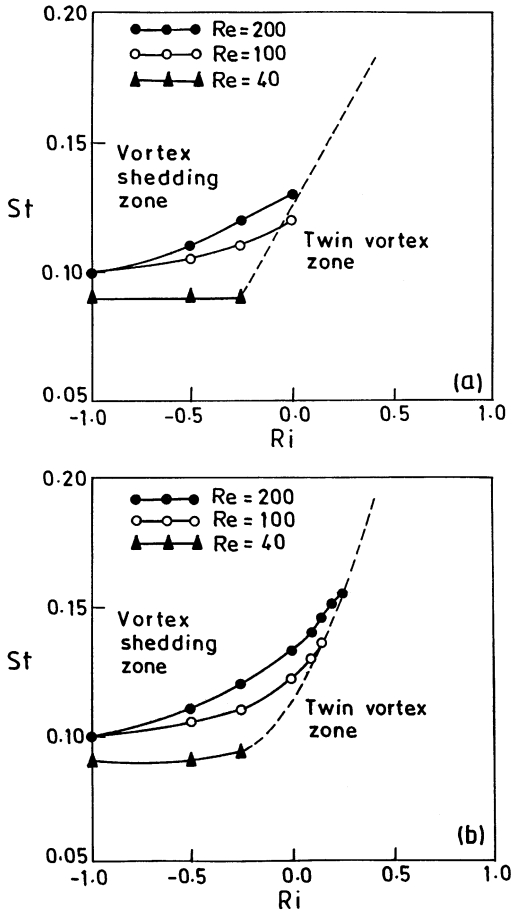


**Figure 12.**
Variation of Strouhal number (St) against Richardson number (Ri) (a) upstream cylinder (b) downstream cylinder

the wake is visualized as revealed by the method of numerical particle releases (NPR). Some conclusions of the present study can be outlined as follows:

- For an isolated circular cylinder, buoyancy opposed convection could trigger the twin vortices naturally formed in the wake region into a "Kármán vortex street" over an Re range of 20 to 40.
- Eddy roll-up process, which exists due to natural shedding over an Re range of 41 to 200, is weakened due to buoyancy aided convection. Here, the dynamic vortices degenerate into twin vortices beyond a certain critical value of Richardson number.
- Zones of vortex shedding and twin eddies are demarcated for flow past a circular cylinder and two cylinders in tandem. Branches of steady state and periodic solutions meet along this boundary, dividing the two zones.
- For two cylinders in tandem, average drag and RMS lift coefficients are presented as a function of Richardson number.

## References

Berger, E. and Wille, R. (1972), "On bluff body wakes", *Annual Reviews of Fluid Mechanics*, Vol. 4, pp. 313-52.

Bourd, R. and Coutanceau, M. (1980), "The early stage of development of wake behind an impulsively started circular cylinder for $40 < Re < 10^4$", *Journal of Fluid Mechanics*, Vol. 101 No. 3, pp. 583-607.

Chang, K.S. and Sa, J.Y. (1990), "The effect of buoyancy on vortex shedding in the near wake of a circular cylinder", *Journal of Fluid Mechanics*, Vol. 220, pp. 253-60.

Chorin, A.J. (1968), "Numerical simulation of Navier-Stokes equations", *Mathematics of Computations*, Vol. 22, pp. 745-62.

Collins, R.J. (1973), "Band width reduction by automatic renumbering", *International Journal for Numerical Methods in Engineering*, Vol. 6, pp. 345-56.

Chilukuri, R. (1987), "Incompressible laminar flow past a transversely vibrating cylinder", *Transactions of ASME Journal of Fluids Engineering*, Vol. 109, pp. 166-71.

Donea, J., Ginliani, S., Laval, H. and Quartapele (1982), "Finite element solution of unsteady Navier-Stokes equations by fractional step method", *Computer Methods in Applied Mechanics and Engineering*, Vol. 30, pp. 53-73.

Eaton, B.E. (1987), "Analysis of laminar vortex shedding behind a circular cylinder by computer-aided flow visualization", *Journal of Fluid Mechanics*, Vol. 180, pp. 117-45.

Eckert, E.R.G. and Soehngen, E. (1952), "Distribution of heat transfer coefficient around circular cylinders in cross-flow at Reynolds numbers from 20 to 500", *Transactions of ASME Journal of Heat Transfer*, Vol. 101, pp. 343-7.

Fletcher, C.A.J. (1984), *Computational Galerkin Methods*, Springer-Verlag, New York, NY.

Hatanaka, K. and Kawahara, M. (1995), "Numerical study of vortex shedding around a heated/cooled circular cylinder by the three-step Taylor-Galerkin method", *International Journal for Numerical Methods in Fluids*, Vol. 21, pp. 857-67.

Igarashi, T. (1981), "Characteristics of the flow around two circular cylinders arranged in tandem-bulletin", *JSME*, Vol. 24 No. 188, pp. 323-31.

Noto, K. and Matsumoto, M. (1985), "A breakdown of the Karman vortex street due to the natural convection", *Flow Visualization*, Vol. 3, p. 348.

Ohya, Y., Okajima, A. and Hayashi, M. (1989), "Wake interference and vortex shedding", in Cheremisinoff, N.P. (Ed.), *Encyclopedia of Fluid Mechanics*, Chapter 10, Vol. 8 on "Aerodynamics and compressible flows", Gulf Publishing company, Houston, TX, pp. 323-89.

Patnaik, B.S.V. (1998), "Finite element analysis of flow past a circular cylinder and two cylinders in tandem: influence of vibration, buoyancy", PhD thesis, IIT, Madras, India.

Patnaik, B.S.V.P., Seetharamu, K.N. and Narayana, P.A.A. (1996), "Simulation of laminar confined flow past a circular cylinder with integral wake splitter involving heat transfer", *International Journal of Numerical Methods for Heat and Fluid Flow*, Vol. 6 No. 4, pp. 65-81.

Perry, A.E., Chong, M.S. and Lim, T.T. (1982), "The vortex shedding process behind two-dimensional bluff bodies", *J. Fluid Mech.*, Vol. 116, pp. 77-90.

Ren, G. and Utnes, T. (1993), "A finite element solution of the time-dependent incompressible Navier-Stokes equations using a modified velocity correction method", *International Journal for Numerical Methods in Fluids*, Vol. 17, pp. 349-64.

Segarlind, L.J. (1984), *Applied Finite Element Analysis*, John Wiley, New York, NY.

Shah, R.K. (1981), "Transient response of heat exchangers", in Kakac, S., Bergles, A.E. and Mayinger, F. (Eds), *Heat Exchangers, Thermal Hydraulic Design*, HemiSphere Publishing Corporation, Washington, DC, pp. 915-53.

Slaouti, A. and Gerrard, J.H. (1981), "An experimental investigation of the end effects on the wake of a circular cylinder towed through water at low Reynolds numbers", *Journal of Fluid Mechanics*, Vol. 112, pp. 297-314.

Slaouti, A. and Stansby, P.K. (1992), "Flow around two circular cylinders by the random vortex method", *Journal of Fluids and Structures*, Vol. 6, pp. 641-70.

Stansby, P.K. and Slaouti, A. (1993), "Simulation of vortex shedding including blockage by the random vortex methods", *International Journal of Numerical Methods in Fluids*, Vol. 17, pp. 1003-13.

Visualized Flow (1988), "Fluid motion in basic engineering situations revealed by flow visualization", compiled by Japanese Society of Mechanical Engineers, Pergamon Press, Tokyo.

Williamson, C.H.K. (1996). "Vortex dynamics in the cylinder wake", *Annual Reviews of Fluid Mechanics*, Vol. 28, pp. 477-539.

Zdrakovich, M.M. (1977), "Review of flow interference between two circular cylinders in various arrangements", *Transactions of ASME Journal of Fluids Engineering*, Vol. 99 No. 4, pp. 618-33.

Zienkiewicz, O.C. and Phillips D.V. (1971), "An automatic mesh generation scheme for plane and curved surfaces by isoparametric co-ordinates", *International Journal of Numerical Methods in Engineering*, Vol. 3, pp. 519-28.